Transition Metal-Free Homopolymerization of Pyrrolo[2,3-d:5,4-d']Bisthiazoles (PBTz) via Nucleophilic Aromatic Substitution (S$_N$Ar)

Somnath Dey,[a] Salahuddin Attar,[a] Eric F. Manley,[b] Salvador Moncho,[a] Edward N. Brothers,[a] Hassan S. Bazzi,[a] Hugo Bronstein,[c] Tobin J. Marks,[b] Martin Heeney,[d] Bob C. Schroeder,*[e] and Mohammed Al-Hashimi,*[a]

[a]Department of Chemistry, Texas A&M University at Qatar, P.O. Box 23874, Doha, Qatar

[b]Department of Chemistry, Materials Research Center, and Argonne-Northwestern Solar Energy Research Center, Northwestern University, 2145 Sheridan Road, Evanston, Illinois 60208, United States.

[c]Department of Chemistry, University of Cambridge, Cambridge CB2 1EW, U.K.

[d]Department of Chemistry and Centre for Plastic Electronics, Imperial College London, Exhibition Rd, London, SW7 2AZ, U.K.

[e]Department of Chemistry, University College London, 20 Gordon Street, London, WC1H 0AJ, U.K.

ABSTRACT Novel methods to synthesize electron-deficient π-conjugated polymers utilizing transition-metal free coupling reactions for the use of non-functionalized monomers are attractive due to their improved atom economy and environmental prospective. Herein, we describe the use of ^{i}PrMgCl·LiCl complex to afford thiazole based conjugated polymers in the absence of any transition metal catalyst, that enabled access to well-defined polymers with good molecular

weights. The mechanistically distinct polymerizations proceeded via nucleophilic aromatic substitution (S_NAr) reaction supported by density functional theory (DFT) calculations. This work demonstrates the first example of fully conjugated thiazole based aromatic homo-polymers without the need of any transition metal catalyst.
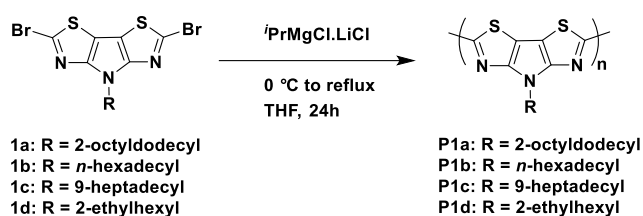
INTRODUCTION Solution-processable conjugated polymeric semiconductors have been widely explored as active materials for lightweight, low cost, flexible plastic electronics.[1-6] Significant developments have been made in the design and synthesis of high performance polymers with charge-carrier mobilities now routinely surpassing 1 cm^2/V.s in organic field effect transistors (OFET) and power conversion efficiencies (PCE) exceeding 15% in photovoltaic devices.[7-12] These breakthroughs have been achieved primarily because of the success of traditional polymerization conditions allowing the synthesis of a wide variety of different types of polymers with good molecular weights. Almost without exception, these methods involve the use of a transition metal catalyst (either Ni or Pd) with appropriately functionalized monomers to undergo either Kumada, Stille or Suzuki coupling polymerizations.[13, 14] Recently, novel methods to synthesize conjugated polymers utilizing C-H activation have emerged which allow for the use of non-functionalized monomers.[15] These methods are attractive due to their improved atom economy but again, these are entirely reliant on transition metal catalyst. The use of transition metal catalysts in synthesis has significant drawbacks both in terms of material property and its use. Residual trace metals in the conjugated polymers can lead to a modification of their properties. A recent example of this is the potential photocatalytic activity of trace palladium in polymers designed for proton reduction.[16, 17] Additionally, it is extremely problematic to both detect and remove trace quantities of these metals.[18] There is also potentially the toxicity associated with

these metals for biological applications of conjugated polymers as well as the intrinsic cost and ecological impact of using them.

From an economical and environmental prospective, it would therefore be beneficial to develop transition-metal free coupling reactions for the synthesis of electron deficient π-conjugated polymers. One possible approach is to employ acid catalyzed aldol condensation chemistry to assemble the π-conjugated backbone.[19] The polymerization is free from transition metal catalysts and therefore much more environmentally friendly. Additional examples of transition metal free polymerization chemistry include the use of the Horner–Wadsworth–Emmons or the Gilch polymerization method to synthesize vinylene linked polymers.[20-22] The use of catalytic amounts of fluoride anions to synthesize high molecular weight poly(p-aryleneethynylene) with low dispersities (Đ),[23-27] which although successful, results in polymers with vinylene linkers, limiting the synthetic scope. Other notable reports include the dehydrative and oxidative cross-coupling methods.[28, 29] Modern high performing conjugated polymers are almost always composed of adjacently linked aromatic rings, and reports of transition metal free polymerizations are rare, particularly with electron deficient aromatics which can be readily oxidatively polymerized.

Herein we outline the use of ^{i}PrMgCl·LiCl complex to afford thiazole containing conjugated polymers from a dibrominated bisthiazole monomer in the absence of any transition metal catalyst. The polymers were obtained in good molecular weights via nucleophilic aromatic substitution (S$_N$Ar) reaction, rather than by transition metal cross-coupling. This work demonstrates the first example of fully conjugated thiazole based aromatic polymers (i.e no vinylene linkages) without the need of any transition metal catalyst.

RESULTS AND DISCUSSION During our initial attempts to explore pyrrolo[2,3-d:5,4-d']bisthiazoles (PBTz) based organotin derivatives using Turbo Grignard (*i*PrMgCl·LiCl), we observed a color change from brown to deep blue. Further investigations showed that after the addition of one equivalent of the *i*PrMgCl·LiCl complex to **1a** (**Scheme 1**) a highly coloured polymeric substance formed upon extended stirring. Intrigued by these initial findings, we further investigated the reaction and underlying mechanism in detail.

1a: R = 2-octyldodecyl
1b: R = *n*-hexadecyl
1c: R = 9-heptadecyl
1d: R = 2-ethylhexyl

P1a: R = 2-octyldodecyl
P1b: R = *n*-hexadecyl
P1c: R = 9-heptadecyl
P1d: R = 2-ethylhexyl

Scheme 1. Synthesis of homopolymers **P1a-P1d**.

First, fused thiazole monomers **1a-d** with various branched amines (2-octyldodecyl, 2-ethylhexyl or 9-heptadecyl) and linear alkyl amine (n-hexadecyl) were prepared.[30-33] Monomers **1a-d** were than treated with 0.9 equivalent of *i*PrMgCl·LiCl at 0 °C, and the reaction mixture was left stirring for 1h at room temperature followed by reflux for 24h to afford the homopolymers **P1a-P1d** in satisfactory yields (**Scheme 1**). The blue polymeric materials **P1a-P1d** were purified by Soxhlet extraction using methanol, acetone, and hexane to remove monomer residues and low molecular weight oligomers. The resulting polymers are all soluble in common organic solvents such as chloroform, and chlorobenzene at room temperature. All the polymers exhibited reasonable degrees of polymerization as determined by size exclusion chromatography (SEC) using 1,2,4-trichlorobenzene at 150 °C. The resulting weight-average (M_w) and number-average (M_n) molecular weights are summarized in **Table 1**. The systematic decrease in molecular weight observed from **P1a** to **P1d** is most likely related to the reducing side chain length and geometry,
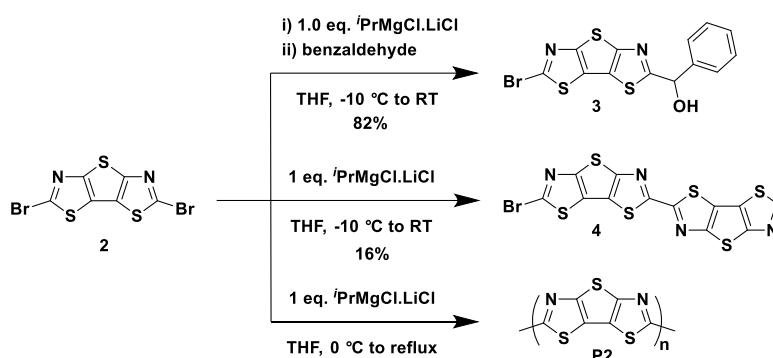
which limits the solubility of higher molecular weight polymers. In an attempt to further optimize the polymerization conditions and improve molecular weights, the amount of Turbo-Grignard added to the PBTz monomer was varied to no avail. Exceeding 1.0 equivalents resulted in the formation of oligomeric PBTz materials, whereas only partially debrominated starting materials were recovered in case less than 0.9 equivalents were used. (< 0.9 equiv.). Using 0.9 equivalents was found to be the ideal ratio to maximise reaction yield and degree of polymerisation.

Table 1. Optical and electrochemical properties of homopolymers **P1a-P1d**.

Polymer	M_n[a] (kDa)	M_w[a] (kDa)	$Đ$ [b]	DP_n[c]	λ_{max}[d] (nm)	IP[e] (eV)	EA[f] (eV)	E^{opt}_g [f] (eV)
P1a	11.6	31.2	2.7	25	618	5.2	3.8	1.5
P1b	5.5	11.5	2.1	14	612	5.3	3.9	1.4
P1c	3.9	6.9	1.7	9	607	5.4	3.9	1.4
P1d	2.6	7.3	2.8	9	599	5.3	3.9	1.4

[a] Determined by SEC (against polystyrene standards) in 1,2,4-trichlorobenzene at 150 °C. [b] Dispersity defined as M_w/M_n. [c] number-average degree of polymerization [d] λ_{max} measured on thin films spin coated from chlorobenzene solution on glass substrate. [e] Ionization potential (IP) calculated by EA – E_g. [f] Electron affinity measured by cyclic voltammetry (E_{red} + 4.8), where E_{red} is the reduction potentials referenced against ferrocene (Fc). The value for Fc with respect to the zero vacuum level is estimated as -4.8 eV. [g] The optical bandgap E^{opt}_g was calculated from the absorption onset, $E^{opt}_g = 1240/\lambda_{onset}$.

We examined the mechanistic aspects of the metalation reaction using a structurally simpler derivative of monomer **1**, 2,6-dibromothieno[2,3-d:5,4-d']bis(thiazole) (**2**), by trapping the Grignard intermediates (**Scheme 2**).
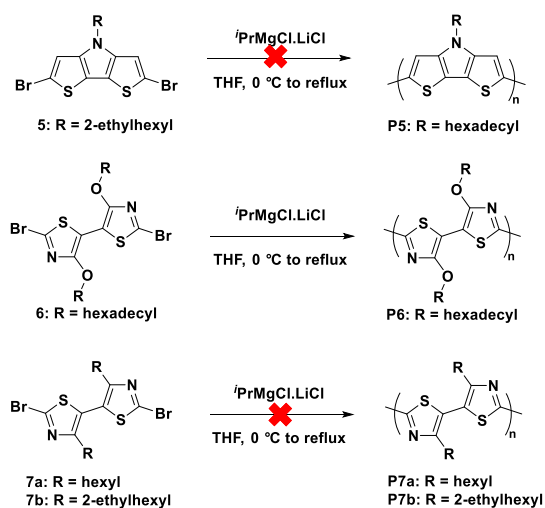

Scheme 2. Mechanistic study of Grignard formation.

Using 1.0 equiv. ^{i}PrMgCl·LiCl resulted in the monometalation of **2**, and the Grignard intermediate was successfully trapped with benzaldehyde to yield (6-bromothieno[2,3-d:5,4-d']bis(thiazole)-2-yl)(phenyl)methanol (**3**) in 82%. In the absence of an external electrophile, dimer **4** was isolated in 16% yield and 74% was attributed to the mono-bromo-substituted PBTz **S12** (see SI). When **2** was reacted with 1 equiv. of ^{i}PrMgCl·LiCl and refluxed in THF, a dark black solid **P2** was isolated, which supports our hypothesis (in the section below) of polymer formation via S$_N$Ar, even though we were at this instance not able to characterize **P2** in more detail due to its complete insolubility.

Subsequently, the synthetic utility of the reaction was explored with different monomers, particularly focusing on the more electron rich dithieno[3,2-b:2',3'-d]pyrrole **5** (DTP), unlikely to undergo S$_N$Ar, and the electron-poor 5,5'-bithiazole derivatives (**6**, **7a** and **7b**). The detailed synthetic routes towards the monomers and their corresponding polymers **P6-P7** are provided in the supporting information, respectively and depicted in **Scheme 3**. Given the different electronic
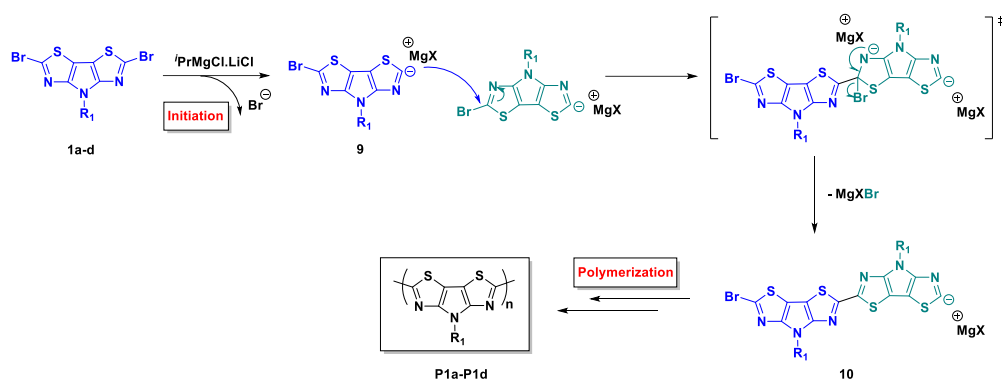
structure of monomers **6**–**7**, we observed significant differences in their respective reactivities. Neither the electron rich monomer **5**, nor the more electron deficient thiazole based monomer **7**, resulted in the formation of polymeric materials. Interestingly, the 2,2'-dibromo-4,4'-bis(hexadecyloxy)-5,5'-bithiazole with its electron donating alkoxy chain yielded the desired target polymer **P6** which warranted a more detailed analysis of the underlying polymerization mechanism.

Scheme 3. Attempted synthesis of bithiazole homopolymer **P6** and **P7**.

Postulated reaction mechanism Based on the experimental data, the following S$_N$Ar reaction mechanism is proposed (**Scheme 4**). The first step (initiation) of the reaction ideally involves the transmetalation at the thiazole unit with the ^{i}PrMgCl.LiCl complex. The Turbo-Grignard would then undergo transmetalation of **1a-d**, resulting in the Br/Mg exchange and the elimination of bromide at 0 °C to form the magnesiated PBTz intermediate **9**. Subsequently, the Grignard species **9** would react with another disubstituted bromo-PBTz monomer **1a-d** affording the corresponding coupled di-PBTz magnesium reagent **10**. We propose sequential S$_N$Ar reactions between the nucleophilic Grignard portion of the molecule and the electrophilic bromine of the thiazoles. It is

unlikely that the metal-halogen exchange selectively forms compound **9**. However, the nature of the reaction mechanism, is such that as long as the overall average stoichiometry of nucleophilic Grignard and electrophilic monomer is approximately 0.9:1, the polymerization will proceed. We attribute the large dispersity of the resulting polymers to be due to the non-selective nature of the Grignard formation which results in a large number of different oligomeric fragments.
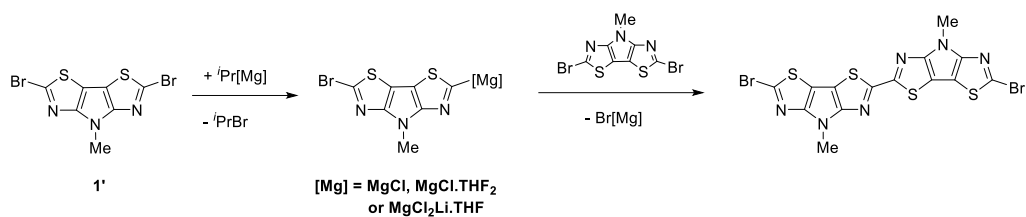

Scheme 4. Proposed S$_N$Ar polymerization reaction mechanism.

While the proposed S$_N$Ar mechanism explains the difference in reactivity observed between monomers **1a-d** and the electron rich monomer **5**, the high reactivity of the alkoxy bithiazole **6** compared to the alkylated counterpart **7** is intriguing. Both bithiazole derivatives are substituted with electron donating substituents, a strong mesomerically donating alkoxy group, and an inductively donating alkyl chain, and therefore should not react readily via S$_N$Ar. S-O interactions, however, are pronounced enough to planarize neighbouring alkoxy bearing thiophene rings and are therefore a popular design criterium to reduce the bandgap in conjugated polymers.[34, 35] Besides, the planarizing effect, this interaction is likely to also have an effect on the mesomerically donating character of the alkoxy substituent. In case of monomer **6**, one of the oxygen lone pair orbitals will interact with the C-S σ* orbital on the adjacent thioazole. As a consequence of the strong S-O interaction, the dihedral angle between the second oxygen lone pair and the thiazole

ring will be restricted, likely reducing its mesomerically donating character and amplifying the inductively withdrawing nature of the O-atom, which would result in monomer **6** being more prone to undergo S$_N$Ar than its alkylated counterparts **7a** and **7b**. In addition, our DFT calculations supports the fact that monomer **6'** prefers to adopt the planar anti-geometry by 3.0 kcal/mol, while monomer **7'** is more stable as a non-planar, syn rotamer by 1.2 kcal/mol.

Density functional theory calculations Density functional theory (DFT) calculations, at the M06L/Def2SVP level in THF were carried out to better understand the rationale behind the experimental results. The polymerization reaction has been calculated according to the mechanism described in **Scheme 5**, which follows a two-step process: (1) the formation of a Grignard reagent and (2) the subsequent polymerization through a S$_N$Ar reaction. The latter is modelled as the formation of a dimer, from a monomer and the Grignard reagent. In all cases, the alkyl side chains on the monomers **1, 5-7** have been substituted with methyl groups to reduce the computational cost. Thus, the model structures are N-methyl-PBTz **1'**, N-methyl-DTP **5'**, 4,4'-dimethoxy-5,5'-bithiazole **6'** and 4,4'-dimethyl-5,5'-bithiazole **7'**. To date the structural information and the full mechanism leading to the synthetically advantageous Turbo Grignard reactant has not yet been fully elucidated.[36] Thus, three different models were used for the preliminary study (**Table S1**) of the structure of the magnesium-containing monomers;[37] the simple divalent magnesium center (-MgCl), the model saturated with solvent (-MgCl.THF$_2$) and with the lithium atom (-MgCl$_2$LiTHF). The results reported here correspond to the magnesium saturated with the solvent model (-MgCl.THF$_2$).

Scheme 5. Chemical structures of the Turbo Grignard reactions analysed here by quantum chemical modelling.

The calculated Gibbs free energies for both steps (the Grignard formation and the dimerization) are summarized in **Table 2**. In all cases, the energies refer to the most stable of the potential rotamers that can be obtained depending on the orientation of the newly formed C-C bond, as well as the internal rotamers for monomers **6'** and **7'**. In general, both the formation of the magnesium intermediate and the dimerization are exothermic processes. However, due to the high activity of the Grignard reactant, this is expected and it is relevant to observe the differences among the species.

Table 2. Calculated free energies of the two reaction steps, according to **Scheme 5.**

ΔG (kcal/mol)	1'	5'	6'	7'
Grignard	-28.3	-25.9	-24.0	-28.5
Dimerization	-59.0	-59.8	-66.6	-57.7
Transition state[a]	27.4	36.7	23.2	25.3

[a] Transition state energy of the dimerization (relative to monomer and Grignard reagent)

In addition, to the reaction mechanism the electron density has been analyzed in the dibrominated monomers and in the Grignard reactants to analyze the effect of their electronic structures in the

S$_N$Ar reaction (**Table 3**). We have obtained the energies of the frontier molecular orbitals and calculated the difference in energy between the HOMO of the nucleophile and the LUMO of the electrophile to assess their interaction. There is a significant agreement between this parameter and the reactivity, with the two reacting monomers having energy differences around 2.6 eV and the non-reacting monomers having differences around 3.0 eV. On the other hand, the calculation of the electron affinity (EA) provides an estimation of the electrophilicity of the monomer. The calculated parameter supports the lack of activity of **5'**, however, insignificant differences are observed among the two bithiazole derivatives **6'** and **7'**.

Table 3. Calculated free energies of the two reaction steps, according to **Scheme 5**.

Species		1'	5'	6'	7'
Monomer	HOMO (eV)	-2.23	-1.69	-2.33	-2.33
	LUMO (eV)	-5.37	-4.89	-4.83	-5.75
	EA (kcal/mol)	37.0	25.9	39.3	39.4
Grignard	HOMO (eV)	-4.92	-4.60	-4.92	-5.38
Complex [a]	Nu$_{HO}$-El$_{LU}$ [b] (eV)	-2.69	-2.91	-2.59	-3.05

[a] This value describes the reaction complex and is calculated from orbitals from the isolated monomer and the Grignard reactant. [b] Nu$_{HO}$-El$_{LU}$ is the difference in energy between the HOMO of the nucleophile (the Grignard reactant) and the LUMO of the electrophile (monomer)

Our calculations suggest that the differences in reactivity for the two pairs or closely related species have different origins. In the case of **1'** and **5'**, the differences in the reaction energies are low (the Grignard formation is 2.4 kcal/mol more favorable in **1'** and the dimerization is 0.8 kcal/mol more

favorable in **5'**), but there is a significant difference in the energy of the transition state for the dimerization (increasing the relative barrier of this step from 27.4 kcal/mol in **1'** to 36.7 kcal/mol in **5'**). The comparison of the transition state geometries suggests an important role of the N-atom, as it forms an additional Mg-N interaction (with a Mg-N distance of 2.646 Å in the transition state of monomer **1'** compared with 2.900 Å Mg-C distance in **5'**) that assists in the cleavage of the Mg-C bond by stabilizing the products as the Mg leaves the carbon atom.
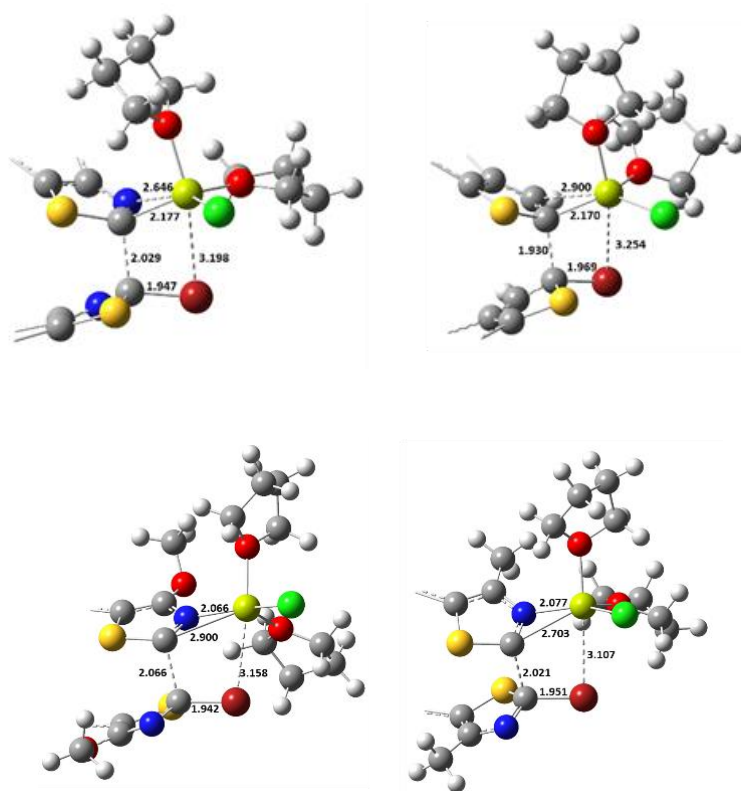

Figure 1. Geometry of the transition state for the monomers with selected bond distances: **1'** (top, left), **5'** (top, right), **6'** (bot-tom, left), **7'** (bottom, right). Focusing in the transition area, only one 5-member ring is depicted for each monomer. Magnesium coordination sphere is saturated with two THF molecules from the solvent. Elements are represented by the following colour scheme: N-blue, C-grey, H-white, O-red, Mg-lime green, S-yellow, Cl-green and Br-maroon.

On the other hand, the differences between the two 5,5'-bithiazole monomers (**6'** and **7'**) seems to be more related to the effects of the methoxy substituent in the geometry. Despite their similarity, both monomers present a different energetically preferred geometry. Meanwhile monomer **6'** prefers to adopt the anti- geometry, which is planar, by 3.0 kcal/mol (compared with a syn geometry, which is not planar), monomer **7'** is more stable as a non-planar, syn rotamer by 1.2 kcal/mol (compared with the planar, anti-geometry). This is attributed to the interaction between the oxygen atom in the methoxy and the sulfur heteroatom. The existence of this interaction can be assessed by the presence of the corresponding bond and ring critical points in the electron density. This effect is more evident when the dimers are formed and it leads to a significant stabilization of the **6'** dimer. Thus, meanwhile the dimerization energies of the four isomers of **7'** are similar (between -53.3 and -57.7 kcal/mol) the preference for the planar anti geometry stabilizes the dimer with alternating rings more than 10 kcal/mol relative to the one with parallel rings. In addition, the dimerization barrier of **6'** is slightly lower than for monomer **7'** (2.1 kcal/mol lower). The methoxy group can contribute to the stabilization of the transition state through the formation of weak interactions between the lone pairs in the O-atom and the ortho hydrogens in the THFs moiety (the O-H shorter distance is 2.676 Å).

The polymers were also simulated as infinite models using periodic boundary conditions (at the HSE06/Def2SVP level of theory in gas phase)[38] and the dimer as the unit cell. From the different possible structures analyzed, based on the relative orientation of the monomer units in either syn- or anti- conformations, all the polymers were found to adopt coplanar conformations as depicted in **Figure 2**. The polymer structure (zigzag) adopting the anti-conformation was calculated to be more stable than the syn-conformation for the rigid structures **P1'** (by 12.1 kcal/mol) and **P5'** (by 10.3 kcal/mol). In the case of **P6'** and **P7'**, numerous orientations are possible due to the rotational

freedom of the monomer around the central σ-bond. However, the most stable geometry corresponds to the anti-orientation of all adjacent thiazole rings, which corresponds to the same orientation of anti-conformation of the monomer (**Figure 2**).
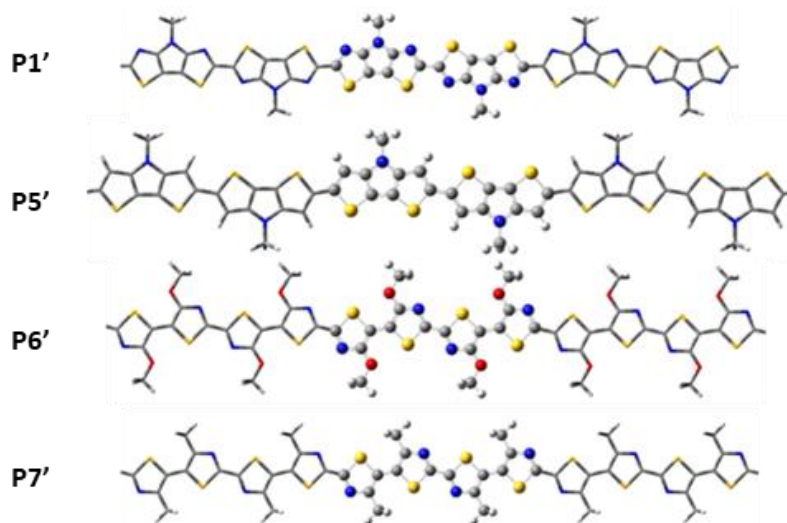

Figure 2. Geometries of the most stable periodic polymer boundaries for the four modelled polymers. "Balls and sticks" representation is used for the atoms included in the periodic cell; "tube" representation is used for the adjacent replicate cells.

DFT and time dependent (TD)-DFT calculations were also performed on the model polymers to examine their optical properties and electronic structure of the newly synthesized polymers (**Table 4**). **Figure S1** shows the spatial distributions of the highest occupied molecular orbital (HOMO) and lowest unoccupied molecular orbital (LUMO) of the optimized polymer. The architecture of the polymers, with substantial coplanarity, consistency with efficient charge transfer in these materials is reflected in both molecular orbital wavefunction distributions, delocalized along the polymer backbone. The calculated energy gap of 1.52 eV for **P1'** (**Table 4**) shows excellent agreement with the experimentally determined values for polymers **P1a-P1d** (**Table 2**). The lowest ten vertical transition energies (Evert) were determined by using TD-DFT (CAM-

B3LYP/Def2SVP)[39] calculations on the octamer system (eight trans-units) in order to reproduce the absorption spectra. The calculated spectra reveal that the dominant energy transition corresponds always to the lowest one with absorptions between 536 and 705 nm with a large oscillator strength (f around 7). The largest orbital contribution of these excitations is from the HOMO to the LUMO.

Table 4. Calculated electronic and optical parameters of the polymers.

	LUMO (eV)	HOMO (eV)	Gap (eV)	E_{vert} (eV)	λ (nm)	f
P1'	-2.91	-4.43	1.52	2.09	592	7.853
P5'	-2.53	-4.12	1.59	2.21	560	7.777
P6'	-3.08	-4.2	1.12	1.76	705	6.681
P7'	-3.24	-5.08	1.83	2.31	536	6.713

f is oscillator strength E_{vert} is vertical transition energies

Homopolymer optical, electrochemical and morphological properties. The optical absorption properties of all PBTz homopolymers were probed via UV-vis spectroscopy in dilute chlorobenzene solution and as thin films (see **Table 1** and **Figure S2**). All the homopolymers exhibited broad absorption bands (450-850 nm) both in solution and thin films, whereas the thin film absorption spectra are slightly blue shifted by up to 26 nm. The similarity of absorption spectra for all the homopolymers both in solution and films suggests that the polymers adopted similar geometries in solution and solid state. By extrapolation of the absorption onsets (λ_{onset}), the optical

bandgaps (E^{opt}_g) of polymers **P1a- P1d** are estimated to be in the range of 1.4 - 1.5 eV, respectively. The ionization potential (IP) and electron affinity (EA) of the polymers were investigated by cyclic voltammetry (CV). All polymers exhibit deep IP of around 5.3 eV, making them inert towards atmospheric oxidation. The out-of-plane X-ray diffraction (XRD) was recorded for polymers **P1a-P1c** to understand the solid-state morphology (**Figure S3**). A weak diffraction peak is observed around 5° for all polymers, indicative of weak lamellar stacking order. However, the low peak intensity shows that while some crystalline intermolecular interactions are pre-sent, they are severely limited in number and size.

CONCLUSION In summary, we report the first synthesis of thiazole based conjugated polymers using nucleophilic aromatic substitution reaction. The use of Turbo-Grignard reagent allowed the substrate activation without employing any transition metal catalysts. Five different homopolymers with various alkyl chains and alkoxy-chain were synthesized. The new polymers exhibit broad absorption bands in the visible spectrum and have low band gaps near 1.4 eV. The presented results demonstrate the feasibility of transition metal-free conjugated polymer synthesis and offer a new and successful synthetic approach to access thiazole based electron deficient polymers.

EXPERIMENTAL SECTION

General. All reactions for monomer synthesis were carried out in oven-dried glassware under an inert atmosphere of dried Argon unless otherwise noted. All chemicals were purchased from Sigma Aldrich or Fisher and used as is. Computational methods and the full synthetic procedures of 4,4'-Dibromo-2,2'-bis(triisopropylsilyl)-5,5'-bithiazole (S1), 2,2'-bis(triisopropylsilyl)-5,5'-bis(hexyl)-bithiazole (S2), 4,4'-Dihexyl-5,5'-bithiazole (S3), 2,2'-bis(triisopropylsilyl)-5,5'-bis(2-

ethylhexyl)-bithiazole (S4), 4,4'-Bis(2-ethylhexyl)-5,5'-bithiazole (S5) leading to **7a/7b,** the synthesis of 4-Methoxythiazole (S7), 4-(hexadecyloxy)thiazole (S8), 4-(hexadecyloxy)-2-(triisopropylsilyl)thiazole (S9), 4,4'-bis(hexadecyloxy)-2,2'-bis(triisopropylsilyl)-5,5'-bithiazole (S10), 4,4'-bis(hexadecyloxy)-5,5'-bithiazole (S11) to afford compound **6** and the procedures for the homopolymerization reactions have been provided in the ESI section.

Synthetic Procedures. *Synthesis of 2,2'-Dibromo-4,4'-dihexyl-5,5'-bithiazole (7a).* To a solution of 4,4'-dihexyl-5,5'-bithiazole **S3** (0.23 g, 0.683 mmol) in anhydrous ether (10 mL), a solution of 2M *n*-BuLi (615 µl, 1.537 mmol) in hexane was added dropwise over 10 min at -78 °C. The reaction mixture was stirred for 1 h, at -78 °C, and a solution of tetrabromomethane (0.57 g, 1.708 mmol) in ether (5 mL) was added dropwise. The reaction mixture was allowed to warm to room temperature overnight. The crude product was diluted with ether (100 mL) and the solid material was removed by filtration. The organic layer was washed with water (100 mL), brine (100 mL), dried over MgSO$_4$ and the solvent was removed under vacuum. The crude product was purified by column chromatography over silica (eluent: hexane/DCM) to afford a dark sticky oil **7a** (0.20 g, 61%). ^{1}H NMR (400 MHz, CDCl$_3$) δ 2.58 (t, [3]$J_{H,H}$ = 7.5 Hz, 4H), 1.63 (m, 4H), 1.21-1.31 (m, 12H), 0.84 (m, 6H). ^{13}C NMR (150 MHz, CDCl$_3$) δ 158.7, 137.5, 126.6, 31.4, 30.1, 29.7, 28.9, 22.5, 14.1. GC-MS calculated for [C$_{18}$H$_{26}$Br$_2$N$_2$S$_2$] 491.99; found 492.30.

Synthesis of 2,2'-Dibromo-4,4'-bis(2-ethylhexyl)-5,5'-bithiazole (7b): The same procedure as **7a** was followed to synthesize **7b**, to afford a solid (0.15 g, 53%). ^{1}H NMR (400 MHz, CDCl$_3$) δ 2.49 (d, [3]$J_{H,H}$ = 7.7 Hz, 4H), 1.83 (m, 2H), 1.19-1.32 (m, 16H), 0.85 (t, [3]$J_{H,H}$ = 6.9 Hz, 6H), 0.78 (t, [3]$J_{H,H}$ = 7.4 Hz, 6H). ^{13}C NMR (150 MHz, CDCl$_3$) δ 157.5, 136.0, 123.1, 39.1, 34.0, 32.5, 28.6, 25.7, 22.9, 14.0, 10.7. GC-MS calculated for [C$_{22}$H$_{34}$Br$_2$N$_2$S$_2$] 548.05; found 548.20.

Synthesis of 2,2'-dibromo-4,4'-bis(hexadecyloxy)-5,5'-bithiazole (6). A mixture of 4,4'-bis(hexadecyloxy)-5,5'-bithiazole **S11** (0.201 g, 0.309 mmol), N-bromosuccinimide (0.24 g, 0.746 mmol), and chloroform (40 mL) was heated in an oil bath at 60 °C for 2 h. The mixture was then concentrated in vacuo, washed with methanol and the resulting solid was purified by column chromatography using 50 % chloroform in hexane as the eluent to afford colorless crystals **6** (0.21 g, 84%). **^{1}H NMR** (400 MHz, CDCl$_3$): δ 4.37 (t, $^3J_{H,H}$ = 6.5 Hz, 4H), 1.81-1.76 (m, 4H), 1.51 – 1.41 (m, 4H), 1.35-1.26 (m, 48H), 0.88 (t, $^3J_{H,H}$ = 6.6 Hz, 6H) ppm. **^{13}C NMR** (150 MHz, CDCl$_3$,): δ 156.4, 131.2, 105.5, 71.6, 31.9, 29.7, 29.7, 29.6, 29.5, 29.4, 29.2, 25.8, 22.7, 14.1 ppm.

CORRESPONDING AUTHOR

Email: mohammed.al-hashimi@tamu.edu; b.c.schroeder@ucl.ac.uk

SUPPORTING INFORMATION Detailed experimental procedures, spectroscopic data and additional DFT data and results are provided.

REFERENCES

1.   Arias, A. C.; MacKenzie, J. D.; McCulloch, I.; Rivnay, J.; Salleo, A., Materials and Applications for Large Area Electronics: Solution-Based Approaches. *Chem Rev* **2010,** *110* (1), 3-24.

2.   Sekitani, T.; Someya, T., Stretchable, Large-area Organic Electronics. *Advanced Materials* **2010,** *22* (20), 2228-2246.

3.   Yokota, T.; Zalar, P.; Kaltenbrunner, M.; Jinno, H.; Matsuhisa, N.; Kitanosako, H.; Tachibana, Y.; Yukita, W.; Koizumi, M.; Someya, T., Ultraflexible organic photonic skin. *Science Advances* **2016,** *2* (4), e1501856.

4.   Huang, S.; Liu, Y.; Zhao, Y.; Ren, Z.; Guo, C. F., Flexible Electronics: Stretchable Electrodes and Their Future. *Advanced Functional Materials* **2019,** *29* (6), 1805924.

5.   Moser, M.; Ponder Jr., J. F.; Wadsworth, A.; Giovannitti, A.; McCulloch, I., Materials in Organic Electrochemical Transistors for Bioelectronic Applications: Past, Present, and Future. *Advanced Functional Materials* **2019,** *29* (21), 1807033.

6.   Zschieschang, U.; Klauk, H., Organic transistors on paper: a brief review. *Journal of Materials Chemistry C* **2019,** *7* (19), 5522-5533.

7.   Paterson, A. F.; Singh, S.; Fallon, K. J.; Hodsden, T.; Han, Y.; Schroeder, B. C.; Bronstein, H.; Heeney, M.; McCulloch, I.; Anthopoulos, T. D., Recent Progress in High-Mobility Organic Transistors: A Reality Check. *Advanced Materials* **2018,** *30* (36), 1801079.

8.   Meng, L.; Zhang, Y.; Wan, X.; Li, C.; Zhang, X.; Wang, Y.; Ke, X.; Xiao, Z.; Ding, L.; Xia, R.; Yip, H.-L.; Cao, Y.; Chen, Y., Organic and solution-processed tandem solar cells with 17.3% efficiency. *Science* **2018,** *361* (6407), 1094-1098.

9.   Wadsworth, A.; Moser, M.; Marks, A.; Little, M. S.; Gasparini, N.; Brabec, C. J.; Baran, D.; McCulloch, I., Critical review of the molecular design progress in non-fullerene electron acceptors towards commercially viable organic solar cells. *Chemical Society Reviews* **2019,** *48* (6), 1596-1625.

10.   Cui, Y.; Yao, H.; Zhang, J.; Xian, K.; Zhang, T.; Hong, L.; Wang, Y.; Xu, Y.; Ma, K.; An, C.; He, C.; Wei, Z.; Gao, F.; Hou, J., Single-Junction Organic Photovoltaic Cells with Approaching 18% Efficiency. *Advanced Materials* **2020,** *32* (19), 1908205.

11.   Lin, Y.; Firdaus, Y.; Isikgor, F. H.; Nugraha, M. I.; Yengel, E.; Harrison, G. T.; Hallani, R.; El-Labban, A.; Faber, H.; Ma, C.; Zheng, X.; Subbiah, A.; Howells, C. T.; Bakr, O. M.; McCulloch, I.; Wolf, S. D.; Tsetseris, L.; Anthopoulos, T. D., Self-Assembled Monolayer Enables Hole Transport Layer-Free Organic Solar Cells with 18% Efficiency and Improved Operational Stability. *ACS Energy Letters* **2020,** *5* (9), 2935-2944.

12.   Liu, Q.; Jiang, Y.; Jin, K.; Qin, J.; Xu, J.; Li, W.; Xiong, J.; Liu, J.; Xiao, Z.; Sun, K.; Yang, S.; Zhang, X.; Ding, L., 18% Efficiency organic solar cells. *Science Bulletin* **2020,** *65* (4), 272-275.

13.   Wu, Z.-Q.; Ono, R. J.; Chen, Z.; Bielawski, C. W., Synthesis of Poly(3-alkylthiophene)-block-poly(arylisocyanide): Two Sequential, Mechanistically Distinct Polymerizations Using a Single Catalyst. *Journal of the American Chemical Society* **2010,** *132* (40), 14000-14001.

14.   Kang, S.; Ono, R. J.; Bielawski, C. W., Controlled Catalyst Transfer Polycondensation and Surface-Initiated Polymerization of a p-Phenyleneethynylene-Based Monomer. *Journal of the American Chemical Society* **2013,** *135* (13), 4984-4987.

15. Pouliot, J.-R.; Grenier, F.; Blaskovits, J. T.; Beaupré, S.; Leclerc, M., Direct (Hetero)arylation Polymerization: Simplicity for Conjugated Polymer Synthesis. *Chem Rev* **2016,** *116* (22), 14225-14274.

16. Kosco, J.; Sachs, M.; Godin, R.; Kirkus, M.; Francas, L.; Bidwell, M.; Qureshi, M.; Anjum, D.; Durrant, J. R.; McCulloch, I., The Effect of Residual Palladium Catalyst Contamination on the Photocatalytic Hydrogen Evolution Activity of Conjugated Polymers. *Advanced Energy Materials* **2018,** *8* (34), 1802181.

17. Kosco, J.; McCulloch, I., Residual Pd Enables Photocatalytic H2 Evolution from Conjugated Polymers. *ACS Energy Letters* **2018,** *3* (11), 2846-2850.

18. Nielsen, K. T.; Bechgaard, K.; Krebs, F. C., Removal of Palladium Nanoparticles from Polymer Materials. *Macromolecules* **2005,** *38* (3), 658-659.

19. Onwubiko, A.; Yue, W.; Jellett, C.; Xiao, M.; Chen, H.-Y.; Ravva, M. K.; Hanifi, D. A.; Knall, A.-C.; Purushothaman, B.; Nikolka, M.; Flores, J.-C.; Salleo, A.; Bredas, J.-L.; Sirringhaus, H.; Hayoz, P.; McCulloch, I., Fused electron deficient semiconducting polymers for air stable electron transport. *Nature Communications* **2018,** *9* (1), 416.

20. Intemann, J. J.; Mike, J. F.; Cai, M.; Barnes, C. A.; Xiao, T.; Roggers, R. A.; Shinar, J.; Shinar, R.; Jeffries-EL, M., Synthesis, characterization, and electroluminescence properties of poly(fluorenevinylene benzobisthiazoles). *Journal of Polymer Science Part A: Polymer Chemistry* **2013,** *51* (4), 916-923.

21. Rittscher, V.; Kuch, S.; Rehahn, M., Gilch Synthesis of Poly(ortho-Phenylene Vinylenes): A Powerful Access to High-Molecular-Weight Blue-Emitting Polymers. *Macromolecular Rapid Communications* **2016,** *37* (10), 814-819.

22. O'Shea, R.; Wong, W. W. H., Simple improvements to Gilch synthesis and molecular weight modulation of MEH-PPV. *Polymer Chemistry* **2020,** *11* (16), 2831-2837.

23. Wang, Y.; Watson, M. D., Transition-Metal-Free Synthesis of Alternating Thiophene−Perfluoroarene Copolymers. *Journal of the American Chemical Society* **2006,** *128* (8), 2536-2537.

24. Dutta, T.; Woody, K. B.; Watson, M. D., Transition-Metal-Free Synthesis of Poly(phenylene Ethynylene)s with Alternating Aryl-Perfluoroaryl Units. *Journal of the American Chemical Society* **2008,** *130* (2), 452-453.

25. Sanji, T.; Iyoda, T., Transition-Metal-Free Controlled Polymerization of 2-Perfluoroaryl-5-trimethylsilylthiophenes. *Journal of the American Chemical Society* **2014,** *136* (29), 10238-10241.

26. Sanji, T.; Motoshige, A.; Komiyama, H.; Kakinuma, J.; Ushikubo, R.; Watanabe, S.; Iyoda, T., Transition-metal-free controlled polymerization for poly(p-aryleneethynylene)s. *Chem Sci* **2015,** *6* (1), 492-496.

27. Sanji, T.; Nose, K.; Kakinuma, J.; Iyoda, T., Transition-metal-free controlled polymerization of 2-polyfluorophenyl-5-trimethylsilylthiophenes: the substituent impact of fluorine. *Polymer Chemistry* **2016,** *7* (46), 7116-7125.

28. Voll, C.-C. A.; Swager, T. M., Extended π-Conjugated Structures via Dehydrative C–C Coupling. *Journal of the American Chemical Society* **2018,** *140* (51), 17962-17967.

29. Gerleve, C.; Studer, A., Transition-Metal-Free Oxidative Cross-Coupling of Tetraarylborates to Biaryls Using Organic Oxidants. *Angewandte Chemie International Edition* **2020,** *59* (36), 15468-15473.

30.   Al-Hashimi, M.; Labram, J. G.; Watkins, S.; Motevalli, M.; Anthopoulos, T. D.; Heeney, M., Synthesis and Characterization of Fused Pyrrolo[3,2-d:4,5-d ']bisthiazole-Containing Polymers. *Org Lett* **2010,** *12* (23), 5478-5481.

31.   Xia, R. D.; Al-Hashimi, M.; Tsoi, W. C.; Heeney, M.; Bradley, D. D. C.; Nelson, J., Fused pyrrolo[3,2-d:4,5-d ']bisthiazole-containing polymers for using in high-performance organic bulk heterojunction solar cells. *Sol Energ Mat Sol C* **2012,** *96* (1), 112-116.

32.   Barłóg, M.; Zhang, X.; Kulai, I.; Yang, D. S.; Sredojevic, D. N.; Sil, A.; Ji, X.; Salih, K. S. M.; Bazzi, H. S.; Bronstein, H.; Fang, L.; Kim, J.; Marks, T. J.; Guo, X.; Al-Hashimi, M., Indacenodithiazole-Ladder-Type Bridged Di(thiophene)-Difluoro-Benzothiadiazole-Conjugated Copolymers as Ambipolar Organic Field-Effect Transistors. *Chemistry of Materials* **2019,** *31* (22), 9488-9496.

33.   Patra, D.; Lee, J.; Lee, J.; Sredojevic, D. N.; White, A. J. P.; Bazzi, H. S.; Brothers, E. N.; Heeney, M.; Fang, L.; Yoon, M.-H.; Al-Hashimi, M., Synthesis of low band gap polymers based on pyrrolo[3,2-d:4,5-d′]bisthiazole (PBTz) and thienylenevinylene (TV) for organic thin-film transistors (OTFTs). *Journal of Materials Chemistry C* **2017,** *5* (9), 2247-2258.

34.   Guo, X.; Quinn, J.; Chen, Z.; Usta, H.; Zheng, Y.; Xia, Y.; Hennek, J. W.; Ortiz, R. P.; Marks, T. J.; Facchetti, A., Dialkoxybithiazole: A New Building Block for Head-to-Head Polymer Semiconductors. *Journal of the American Chemical Society* **2013,** *135* (5), 1986-1996.

35.   Thorley, K. J.; McCulloch, I., Why are S–F and S–O non-covalent interactions stabilising? *Journal of Materials Chemistry C* **2018,** *6* (45), 12413-12421.

36.   Li-Yuan Bao, R.; Zhao, R.; Shi, L., Progress and developments in the turbo Grignard reagent i-PrMgCl·LiCl: a ten-year journey. *Chemical Communications* **2015,** *51* (32), 6884-6900.

37.   Krasovskiy, A.; Straub, B. F.; Knochel, P., Highly Efficient Reagents for Br/Mg Exchange. *Angewandte Chemie International Edition* **2006,** *45* (1), 159-162.

38.   Heyd, J.; Scuseria, G. E., Efficient hybrid density functional calculations in solids: Assessment of the Heyd–Scuseria–Ernzerhof screened Coulomb hybrid functional. *The Journal of Chemical Physics* **2004,** *121* (3), 1187-1192.

39.   Yanai, T.; Tew, D. P.; Handy, N. C., A new hybrid exchange–correlation functional using the Coulomb-attenuating method (CAM-B3LYP). *Chemical Physics Letters* **2004,** *393* (1), 51-57.